Bone 50 (2012) 581–591

Contents lists available at SciVerse ScienceDirect

Bone

journal homepage: www.elsevier.com/locate/bone

Original Full Length Article

Mechanical Stretch Induced Calcium Efflux from Bone Matrix Stimulates Osteoblasts☆

Xuanhao Sun [a], Eric McLamore [b,1], Vipuil Kishore [c], Kateri Fites [a], Mikhail Slipchenko [a], D. Marshall Porterfield [a,b], Ozan Akkus [c,*]

[a] Weldon School of Biomedical Engineering, Purdue University, West Lafayette, IN 47907, USA
[b] Department of Agricultural and Biological Engineering, Purdue University, West Lafayette, IN 47907, USA
[c] Department of Mechanical and Aerospace Engineering, and Biomedical Engineering, Case Western Reserve University, Cleveland, OH 44106, USA

ARTICLE INFO

Article history:
Received 11 August 2011
Revised 1 December 2011
Accepted 19 December 2011
Available online 29 December 2011

Edited by: David Burr

Keywords:
Calcium efflux
Bone matrix
Damage targeting
Mechanochemical transducer
Intracellular calcium
Osteoblast

ABSTRACT

The mechanisms by which bone cells sense critically loaded regions of bone are still a matter of ongoing debate. Animal models to investigate response to microdamage involve *post mortem* immunohistological analysis and do not allow real-time monitoring of cellular response during the emergence of the damage in bone. Most *in vitro* mechanical stimulation studies are conducted on non-bone substrates, neglecting the damage-related alterations in the pericellular niche and their potential effects on bone cells. The current study reports spontaneous efflux of calcium ions (Ca^{2+}) (1.924 ± 0.742 pmol $cm^{-2}\,s^{-1}$) from regions of devitalized bone matrix undergoing post-yield strains, induced by a stress concentrator. When these samples are seeded with MC3T3-E1 osteoblasts, the strain-induced Ca^{2+} efflux from bone elicits cell response at the stress concentration site as manifested by activation of intracellular calcium signaling (increase in fluorescence by $52\% \pm 27\%$). This activity is associated with extracellular calcium because the intracellular calcium signaling in response to mechanical loading subsides when experiments are repeated using demineralized bone substrates (increase in fluorescence by $6\% \pm 10\%$). These results imply a novel perspective where bone matrix acts as an intermediary mechanochemical transducer by converting mechanical strain into a chemical signal (pericellular calcium) to which cells respond. Such a mechanism may be responsible for triggering repair at locations of bone matrix undergoing critical deformation levels.

1. Introduction

Bone sustains microfractures physiologically due to fatigue and supraphysiologically due to overload episodes [1–3]. Cell-mediated repair of bone is preferentially associated with such critically loaded regions of bone, suggesting that bone cells can target damage for repair [4]. Response of bone cells to damage are mostly studied by animal models [5,6] which usually involve *post hoc* immunohistological analysis but do not allow real-time monitoring of cellular response during the emergence of the damage in bone. To this date, there are no *in vitro* damage models which allow studying bone cells in response to damage formation within bone matrix. Most studies on stimulation of bone cells are conducted on non-bone synthetic substrates; therefore, if alterations in the pericellular physicochemical environment are stimulant to bone cells, such effects have not been investigated. There has been little focus on indirect pathways wherein mechanical loading may come to affect bone cells' response by altering the chemistry of their pericellular niche in bone matrix.

Sliding between collagen fibrils [7], disruption of sacrificial ionic bonds [8], and intergranular friction [9] have been proposed to occur at the nanoscale of bone upon loading. A recently developed experimental model in our laboratory introduces notches (i.e. stress raisers) to bone slices to amplify mechanical stress controllably in a site-specific fashion which allows for real-time observation of the evolving damage *in vitro* [10]. Upon the emergence of a damage zone in this model, we observe a mechanically-induced exposure of nanostructural features of the same length scale with mineral crystals of bone and of positive charges similar to the calcium moieties in bone during post-yield deformation [10,11]. Based on this hindsight we hypothesize that mechanical strain induces an efflux of calcium ions (Ca^{2+}) from bone matrix to the pericellular space. If exists, such an efflux would not be one without any consequences because it has been well documented that changes in the concentration of extracellular Ca^{2+} ($\mathbf{[Ca_o^{2+}]}$) regulates a wide range of biological activities, such as secretion [12], muscle contraction [13] and

☆ **Disclosures:** All authors state that they have no conflicts of interest.

* Corresponding author at: Mechanical and Aerospace Engineering, Biomedical Engineering, Case Western Reserve University, 10900 Euclid Ave., Cleveland, OH 44106, USA.
E-mail addresses: xuanhao@purdue.edu (X. Sun), emclamor@ufl.edu (E. McLamore), vipuil.kishore@case.edu (V. Kishore), kfites@purdue.edu (K. Fites), mslipche@purdue.edu (M. Slipchenko), porterf@purdue.edu (D.M. Porterfield), ozan.akkus@case.edu (O. Akkus).
[1] Currently at: Department of Agricultural and Biological Engineering, University of Florida, Gainesville, FL 32611, USA.

8756-3282/$ – see front matter © 2011 Elsevier Inc. All rights reserved.
doi:10.1016/j.bone.2011.12.015

neurotransmission [14]. There is also evidence that increased levels of $\mathbf{Ca_o^{2+}}$ stimulate osteoblasts [15,16] and osteocytes [17,18]. Based on the documented responsiveness of bone cells to $\mathbf{Ca_o^{2+}}$, we hypothesized further that mechanically-induced calcium efflux from bone matrix is stimulant to bone cells.

The first hypothesis was tested by measuring the Ca^{2+} efflux from devitalized bone surface in real-time during mechanical loading. After the confirmation of a significant level of Ca^{2+} efflux from bone at critically-strained regions, we investigated the response of mouse calvarial osteoblasts (MC3T3-E1) seeded on bone substrates subjected to loading, and the change in intracellular Ca^{2+} concentration ($\mathbf{[Ca_i^{2+}]}$) was monitored in real-time by using intracellular calcium indicators. Demineralized bone samples were used as a negative control to assess cellular response to substrate stretch alone without the Ca^{2+} efflux. Furthermore, to completely decouple the potential effects of Ca^{2+} efflux and substrate strain on activating bone cells, MC3T3-E1 cells were seeded onto porous substrates and subjected to the Ca^{2+} efflux from apical and basal (i.e. substrate) aspects.

2. Materials and Methods

2.1. Bone sample preparation

Block beams from bovine femurs were prepared using a low-speed diamond blade saw (Buehler Ltd., Lake Bluff, IL) (Fig. 1A). A V-notch (notch root radius ~ 100 μm), extending half the depth of the remaining cortical thickness was introduced through the center of the beam using a mill (Series 5400, Sherline, Vista, CA). Block beams were sectioned into thin wafers (0.2 mm), and polished with progressively finer grades of 600, 800, and 1200 grade polishing paper (Buehler Ltd., Lake Bluff IL) and fine alumina powder (0.3 μm). Sonicator (Model FS20, Fisher Scientific, Waltham, MA) was used to remove the polishing debris between each polishing step (2 minutes for each sonification period). The final dimensions of the notched wafer were approximately 50 × 4 × 0.2 mm. A final sonication stage was performed to remove any remaining polishing and cellular debris from the devitalized bone surface. Polished wafers are stored in a −20 °C freezer upon using.

2.2. Tensile test of devitalized bone under light microscope in the absence of cells

Samples were loaded at a rate of 6 μm/s using a miniaturized tensile test device (Ernest F. Fullam Inc, Troy, NY, USA) which was fixed on the stage of a light microscope (BX51, Olympus America) (Figs. 1B, C). This microscope setting allowed both transmission and reflection images to be taken during the loading process (Fig. 1D). A UV epifluorescent light source was used when imaging the fluorescent indicators. During the entire tensile test, strips of Kimwipe were draped over the samples. These strips kept the bone partially wet by wicking in water from the reservoir below the specimen. The overall humidity in the region of testing was maintained around 60% by a humidifier.

2.3. Calcium indicator staining for visual confirmation of ionized calcium exposure

Calcium indicator, Fluo-4FF (F23980, Invitrogen) was used to confirm calcium exposure during damage evolution. Samples were presoaked with calcium indicator for 15 minutes, and then loaded until the emergence of the opaque process zone at the notch root (about 0.2-0.5% (with an average of 0.3%) tissue level strain or 20 newtons in loading, for the given sample geometry), and held at the loaded state for 15 more minutes to provide time for stain penetration and interaction with calcium ions. Sample was unloaded and calcium indicator solution on the bone surface was blown away by duster air before UV epifluorescent images were taken. Three specimens were tested to confirm the repeatability of the reported results.

2.4. SHG image and fluorescent image of process zone

Second harmonic generation (SHG) images of mineralized collagen fibers were obtained and overlaid with two-photon excited fluorescence (TPEF) images of the damage stained by a negatively charged dye, Dextran AlexaFluor488, which we have shown to label the damage in the process zone earlier [10]. SHG and TPEF images were acquired using an inverted confocal microscope (FV1000 + IX81, Olympus America Inc, PA) equipped with a mode-locked femtosecond Ti: Sapphire laser (Mai Tai, Spectra-Physics, Fremont, CA). The

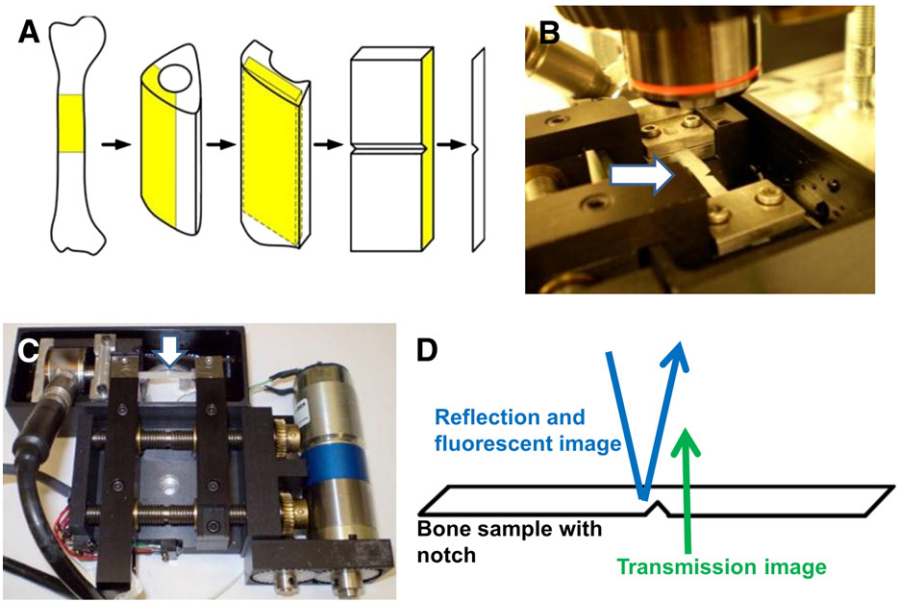

Fig. 1. Sample preparation and experimental setup. (A) Schema of wafer specimen preparation. (B) Samples were loaded using a miniaturized tensile test device which was fixed on the stage of a light microscope. (C) The device loads the sample symmetrically, maintaining the point of interest in the field of view during loading. White arrow points at bone specimen. (D) The schema represents the reflection fluorescence illumination light pathway (blue arrow) and the transmission illumination light pathway (green arrow).

average excitation power at the sample was approximately 30 mW with an excitation wavelength of 840 nm. A 60x water immersion objective (1-U2B893IR, 1.2 numerical aperture, Olympus) was used to focus laser beam into the specimen. The SHG signal was collected by the same objective and directed towards backward external photomultiplier tube (PMT) detector mounted at the side port of the microscope. The dichroic mirror (650dcspxr, Chroma, VT) was used to separate detected SHG signals from the excitation beam. The TPEF signals was collected in the forward direction by air condenser (IX2-LWUCD, 0.55 numerical aperture, Olympus) and directed towards forward external PMT detector (both external PMTs are model R7683 from Hamamatsu Photonics, Japan). The 430/40 and 520/70 bandpass filters (Chroma, VT) were used in front of PMTs to selectively detect SHG and TPEF signals, respectively. Each acquired image (512×512 pixels) covered an area of $120\times120\ \mu m^2$ and was integrated over 3 frames to improve signal to noise ratio. SHG image was pseudo-red colored and overlapped with TPEF image in ImageJ.

2.5. Calcium Efflux Measurement by Self-referencing (SR) Calcium Microsensor

Ion-selective microelectrodes (ISE) were used to measure calcium efflux and concentration. ISE were constructed using non-filamented 1.5 mm borosilicate glass capillaries (World Precision Instruments) pulled on a Sutter P-97 horizontal puller (Flaming-Brown, Sutter instrument Co) to obtain a shank of about 4.0 mm and a tip diameter of approximately 2–5 μm. ISE utilized an immobilized liquid exchange membrane and an Ag/AgCl reference electrode. Immediately prior to use, microelectrodes were backfilled with electrolyte and then front filled with ion exchange cocktail (Ionophore). Microelectrodes were inserted into a half-cell microelectrode holder fitted with an electrolitically plated Ag/AgCl wire. The return pathway (reference probe) for the circuit was 3 M KCl immobilized in 3% agar injected into 1.5 mm polyethylene tubing inserted in a microelectrode holder half cell (World Precision Instruments). SR hardware included a vibration isolation table with Faraday cage (Technical Manufacturing Co), camera/zoomscope and sensor mounted on a head stage controlled by a motion control system. Automated Scanning Electrode Technique (ASET) software was used for data acquisition and control functions (Science Wares) (Fig. 2A).

The SR technique compensates for the errors introduced by ambient drift and noise by oscillating between two locations (termed near pole and far pole) at a fixed excursion distance (50 μm). The differential concentration ($\Delta[Ca^{2+}]$) had approximately linear dependence ($R^2=0.98$) on excursion distance (Δx) for small Δx, enabling calculation of flux using Fick's first law of diffusion (the molecular diffusion coefficient $D=4.5\times10^{-5}\ cm^2\ sec^{-1}$) [19]. The values of $[Ca^{2+}]_1$ and

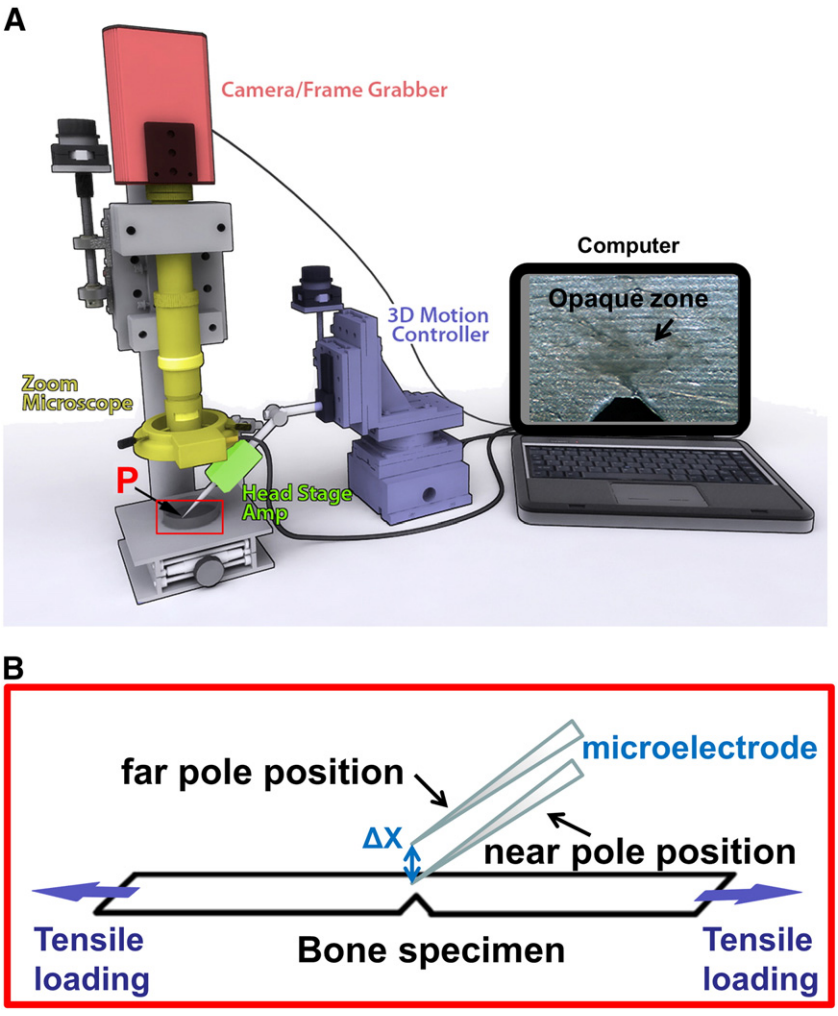

Fig. 2. Self-referencing microsensor to measure Ca^{2+} efflux. (A) Self-referencing system consisted of camera/zoomscope and sensor mounted on a head stage controlled by a motion control system. P indicates the tip of the electrode; Red inset highlights the sample location. (B) Enlarged diagram of the red inset in A: calcium efflux is measured at notch root in real-time while bone specimen is under tensile loading, with microelectrode oscillating between far pole and near pole positions (not drawn to scale).

$[Ca^{2+}]_2$ are calculated by the ASET software using the following equations:$[Ca^{2+}]_1 = 10^{E_1 - b/s}$;$[Ca^{2+}]_2 = 10^{E_2 - b/s}$, where E_1 and E_2 are potentials measured at near pole, and far pole, respectively (mV), b is y-intercept of the Nernst plot (mV), and s is the slope of the Nernst plot (mV $\log[H^+]^{-1}$). The Ca^{2+} flux was calculated by using equation:

$$J = -D\left(\frac{\left(10^{E_1 - b/s} - 10^{E_2 - b/s}\right)}{\Delta x}\right),$$

where J is the Ca^{2+} flux (nmol cm^{-2} s^{-1}), Δx the excursion distance between near/far pole (50 μm) (Fig. 2B).

The miniaturized tensile test device was mounted on the stage of the microsensor system. The microelectrode was positioned above the bone surface within 5 μm during measurements. Measurement was conducted with bone immersed in 1X PBS (GIBCO). Temporal changes in Ca^{2+} concentration and efflux were measured in real-time at the root of the notch in bone before loading, during loading (until the emergence of the opaque process zone at about 20 N), and after the removal of loading (N = 5). Experiments were repeated with bone being immersed with $CaCl_2$ (2 mM) supplemented PBS as well.

2.6. Observations of the Osteoblasts Seeded on Devitalized Bone

To assess whether Ca^{2+} efflux from loaded bone is stimulant to bone cells, we seeded the mouse calvarial osteoblastic cells (MC3TC-E1 subclone 4, ATCC) on notched bone samples and repeated the mechanical tests to observe their response. Cells were cultured in α-MEM (GIBCO) containing 10% FBS (GIBCO), 60 Unit/ml penicillin/streptomycin and 1.5 μg/ml Fungizone and maintained at 37 °C and 5% CO2 in a humidified incubator. Notched bone specimen was prepared the same way as described before, and sterilized in 70% EtOH overnight. EtOH was rinsed with PBS (GIBCO) and left for drying in the in the laminar hood for 20 min. This was repeated for 3 times to ensure the complete removal of EtOH. MC3T3-E1 cells were seeded on the sterilized bone at a density of 20,000 cells per cm^2 with culture media overnight (i.e. cells covered the entire bone surface).

Demineralized samples (N = 4) were used as a negative control (substrate stretch without Ca^{2+} efflux). Molten bee's wax was used to coat grip regions of the bone specimen (the outer one third regions) which masked the grip regions from demineralization. The mid portion of the sample including the notch area was otherwise exposed to ensuing demineralization treatment (about 4 mm in length). After bee wax solidified, the bone specimen was immersed in 0.5 M ethylenediaminetetraacetic acid (EDTA, Sigma) for 5 hours with moderate agitation. Demineralization was confirmed by the disappearance of PO_4^{3-} peak by Raman spectroscopy and the bee's wax on the specimen is gently peeled off with the assistance of a razor blade. Specimen sterilization and cell seeding procedure for the demineralized bone was the same as the undemineralized bone afterwards. The cell seeding and attachment onto both undemineralized and demineralized bone was confirmed by Alexa Fluor 488 phalloidin (Invitrogen) for F-actin stain.

Since elevated intracellular Ca^{2+} concentration ($\mathbf{[Ca_i^{2+}]}$) has been shown to trigger a wide range of downstream cellular events [20,21] and can be easily monitored in real-time with intracellular calcium indicators, $\mathbf{[Ca_i^{2+}]}$ has been widely used as an early signal to study bone cells during mechanotransduction [22,23]. Fluo-4 AM calcium indicator was used to monitor the cellular response in terms of the change in $\mathbf{[Ca_i^{2+}]}$. Cells were incubated with 0.5 μM Fluo-4 AM for 90 min before real-time $\mathbf{[Ca_i^{2+}]}$ monitoring during mechanical loading. Cell-seeded notched bone specimens were loaded at a rate of 6 μm/s until the emergence of the opaque process zone (0.2%-0.5% (with an average of 0.3%) tissue level strain or about 20 newtons in loading) using the miniaturized tensile stage setup under the microscope (N = 4) [10]. The bath medium has 1.8 mM baseline $[Ca^{2+}]$ background in α-MEM + 1%FBS, with no additional Ca^{2+} added. Demineralized samples (N = 4) were loaded at least twice the strain (1%-6% (with an average of 3.8%) tissue level strain or about 2 newtons in loading) experienced by undemineralized specimen to ensure cells seeded on demineralized bone were subjected to no less substrate deformation than that of the undemineralized samples.

2.7. Activating cells with mimicked calcium efflux in the absence of mechanical loading

Demineralized samples discounts calcium contribution; however, the presence of substrate stretch was present. To completely decouple the potential effects of Ca^{2+} efflux and substrate strain on activating bone cells, MC3T3-E1 cells were seeded onto porous substrates (0.4 μm culture plate insert, Corning). To mimic the Ca^{2+} efflux from bone (calcium efflux from bone incident on cells from their basal aspect), 1.2 mL media underneath the cell-seeded inserts was replaced with media containing 10X, 100X, or 1000X of baseline $CaCl_2$ concentration in the αMEM media (1X = 1.8 mM), while the media above the insert was unaltered. This generated a Ca^{2+} gradient across the insert, resulting in Ca^{2+} efflux toward the cells, mimicking the Ca^{2+} efflux from bone substrate. Therefore, the only stimulus applied to MC3T3-E1 cells was the Ca^{2+} efflux from below the substrate (basal side) without any confounding substrate deformation. To compare with the cellular response to the Ca^{2+} efflux from the apical side, experiment was repeated with cells seeded directly at the bottom of the culture wells (with 1.8 mM baseline $[Ca^{2+}]$ in medium) and $CaCl_2$ added directly from the above (medium was replaced with 10X, 100X, or 1000X $CaCl_2$ supplemented medium, 0.75 ml was added to keep the height of the medium above the cells as the same as that in the insert group) (Fig. 3). Both substrates were cell adhesion optimized synthetic polymer surfaces: the porous insert is made from polyester (PET), while the culture well is made from polystyrene. Cells have adhered to both types of surfaces without any

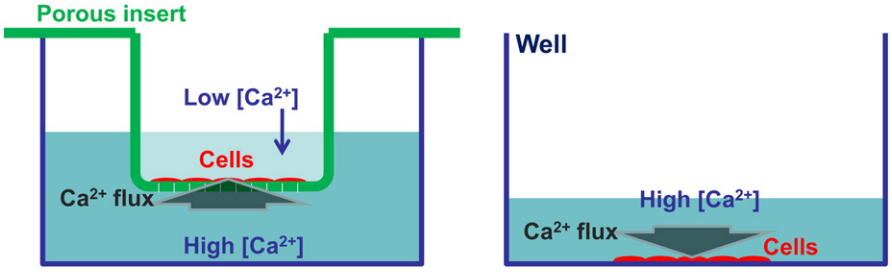

Fig. 3. Cells seeded on porous insert (Left) to mimic the Ca^{2+} efflux from basal substrate aspect, while cells seeded on well (Right) to mimic Ca^{2+} flux from the apical aspect of cells.

apparent differences in cytoskeletal morphology compared with cells seeded on bone (confirmed Alexa Fluor 488 phalloidin).

2.8. Activating cells with osmotic pressure with glucose-supplemented media

To investigate the potential role of osmotic pressure from the $CaCl_2$ supplemented media on activating the osteoblasts, we conducted additional experiments with bath medium supplemented with 540 mM glucose which creates an osmotic pressure equivalent of 180 mM $CaCl_2$. In this way we provided a similar osmotic pressure in the absence of calcium. Glucose-supplemented media were applied in both osteoblast-seeded porous insert and culture well the same way as described above in section 2.7. The results were compared with that from the $CaCl_2$-supplemented media group using an inverted microscope.

2.9. Data recording and analysis

Fluorescence images were recorded at 2 fps by a CMOS (Infinity, Lumenera) on the upright microscope, or 0.2 fps by a CMOS (Q-color 5, Olympus) on the inverted microscope, and analyzed by ImageJ (NIH). For cell-seeded bone loading experiments, four samples each from undemineralized bone or demineralized bone group were tested and ten most discernable cells on each sample were analyzed. Nested-ANOVA was used to compare the peak fluorescence level over pre-loading baseline level between cells seeded on original bone and demineralized bone. Fluorescence was plotted after normalization by pre-load baseline fluorescence level. For cell-seeded insert or well experiments, 10 cells each at different $CaCl_2$ level on either insert or well were analyzed. Student's *t* test was used to compare the peak fluorescence between cells seeded on insert and on well at each applied $CaCl_2$ level and baseline fluorescence level before $CaCl_2$ was added. Time-course fluorescence figures were plotted after normalizing their baseline fluorescence to the same level to facilitate comparison between different groups. The significance of the $CaCl_2$ concentration effect on the cell fluorescence response was tested by ANOVA on the slope of linear regression fit. Experiments with glucose-supplemented media were analyzed the same way as those with $CaCl_2$-supplemented media. Student's *t* test was used to compare the peak fluorescence between glucose-supplemented experiments and $CaCl_2$-supplemented experiments.

3. Results

3.1. Exposure of calcium-rich moieties of bone during mechanical loading

Upon mechanical loading, elevated fluorescence intensity was observed at the notch root of devitalized bone samples soaked in Fluo-4FF prior to loading. Fluorescent regions overlapped with the damage process zone (manifested by an opacity emerging at notch root [10]) observed using the transmission mode (Figs. 4A, B). This result indicates that the Ca^{2+}-rich regions of bone are exposed at the notch root upon mechanical loading. Overlay of collagen fiber orientation obtained by second harmonic generation (SHG) (Fig. 4C) with stain-labeled damage patterns demonstrate both extrafibrillar (generally delamination between fibers) and intrafibrillar (damage traversing fibers obliquely) interactions between collagen fibers and the damage.

3.2. Efflux of Ca^{2+} from bone measured by SR Calcium Microsensor

An immediate elevation of both Ca^{2+} concentration and efflux was observed concomitant with the mechanical loading and the emergence of the opaque zone (N = 5). Efflux levels returned to the baseline level upon the removal of mechanical loading (Fig. 5). The baseline Ca^{2+} efflux before mechanical loading (0.120 ± 0.083 pmol $cm^{-2}\,s^{-1}$, avg. ± st.dv.) increased 16-fold (1.924 ± 0.742 pmol $cm^{-2}\,s^{-1}$) at the emergence of yield zone and dropped back to the preloading level upon unloading (0.561 ± 0.145 pmol $cm^{-2}\,s^{-1}$) (Fig. 5D). In experiments repeated with 2 mM $CaCl_2$, no change in efflux or concentration upon mechanical loading was observed (data not shown).

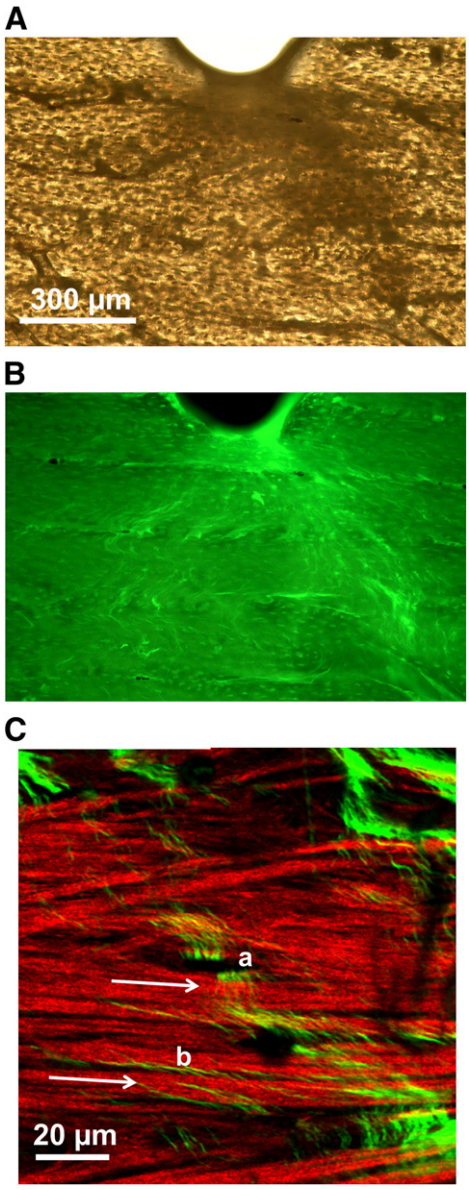

Fig. 4. Representative transmission, fluorescence and second harmonic generation (SHG) images. (A) Display of the "process zone" forming at the notch tip with transmission illumination. (B) Elevated fluorescence intensity at process zone (shown in A) after being pre-soaked with calcium indicator, Fluo-4FF, and then mechanically loaded. (C) Process zone fluorescence image (green) overlapped with SHG image of collagen fibrils in bone (pseudo-red-colored). Stain uptake occurs both perpendicular (labeled by a, within intrafibrillar space) and parallel (labeled by b, within extrafibrillar space) to the orientation of collagen fibrils (arrows).

3.3. Activation of bone cells by mechanically-induced calcium efflux from the bone matrix

Staining for the cytoskeleton for F-actin (Alexa Fluor 488 phalloidin) showed that MC3T3-E1 cells attached to both undemineralized bone and demineralized bone, and there were no differences in the cell seeding density or morphology of the cytoskeletons of the attached cells

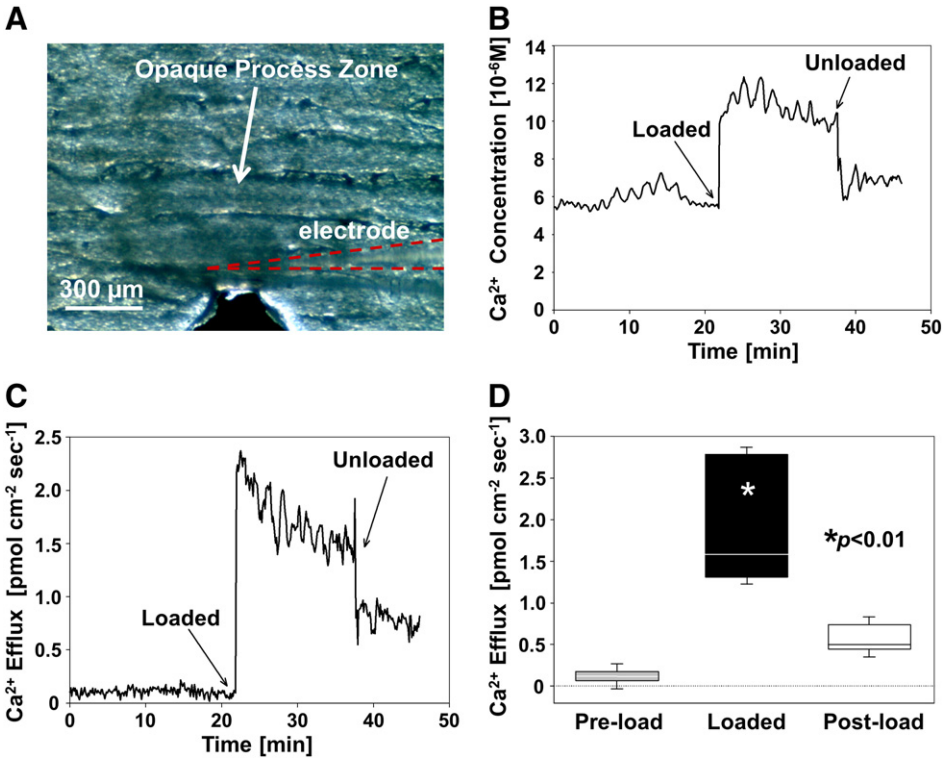

Fig. 5. Real-time Ca^{2+} measurement at bone surface during mechanical loading. (A) Microelectrode (dashed red line) was above an opaque process zone (arrow) during measurement. (B) Representative Ca^{2+} concentration levels. (C) Representative Ca^{2+} efflux levels. (D) Difference in the Ca^{2+} efflux levels at different loading states (*:Ca^{2+} efflux level upon mechanical loading is significantly higher than the rest, $p<0.01$).

(Figs. 6A, B). Upon mechanical loading of undemineralized bone, MC3TC-E1 cells stained with Fluo-4 AM increased their intracellular calcium fluorescence intensity by about 50% ($F_{increase}/F_{baseline}$: 52% ± 27%, N = 40), while the cells seeded on demineralized bone showed significantly diminished response ($F_{increase}/F_{baseline}$: 6% ± 10%, N = 40) upon loading (Figs. 6C, D).

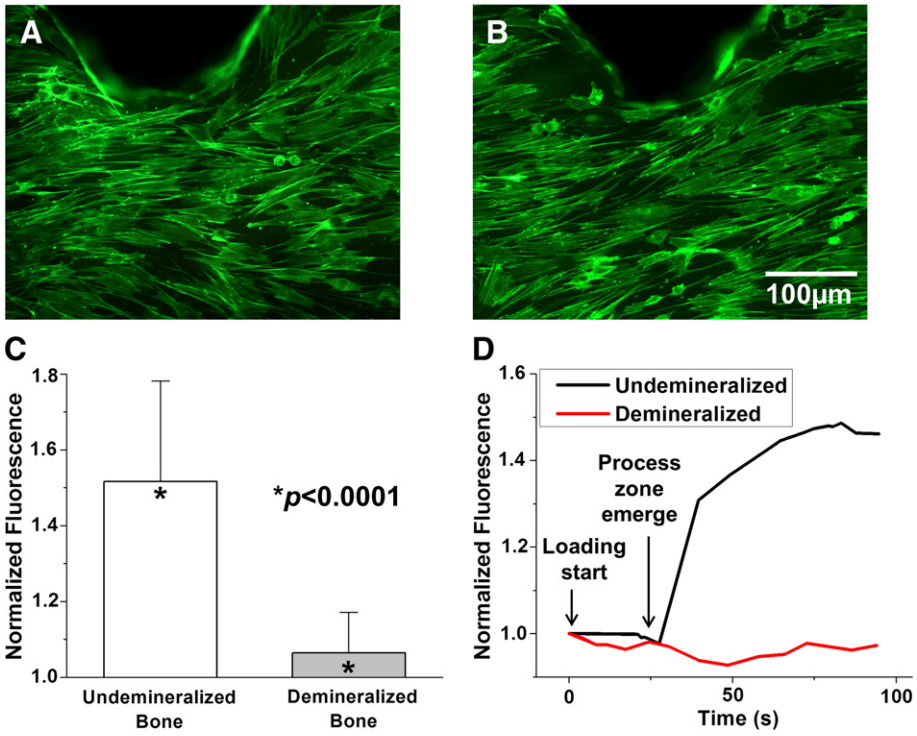

Fig. 6. Activation of MC3T3-E1 by mechanically-induced calcium efflux from bone. MC3T3-E1 cells' attachment stained with Alexa Fluor 488 phalloidin (F-actin) on undemineralized bone (A) and on demineralized bone (B). (C) Comparison of fluorescence increase in MC3T3-E1 cells seeded on undemineralized bone and demineralized bone upon mechanical loading. (D) Representative curves of temporal change in fluorescence intensity of a single cell seeded on undemineralized bone and on demineralized bone.

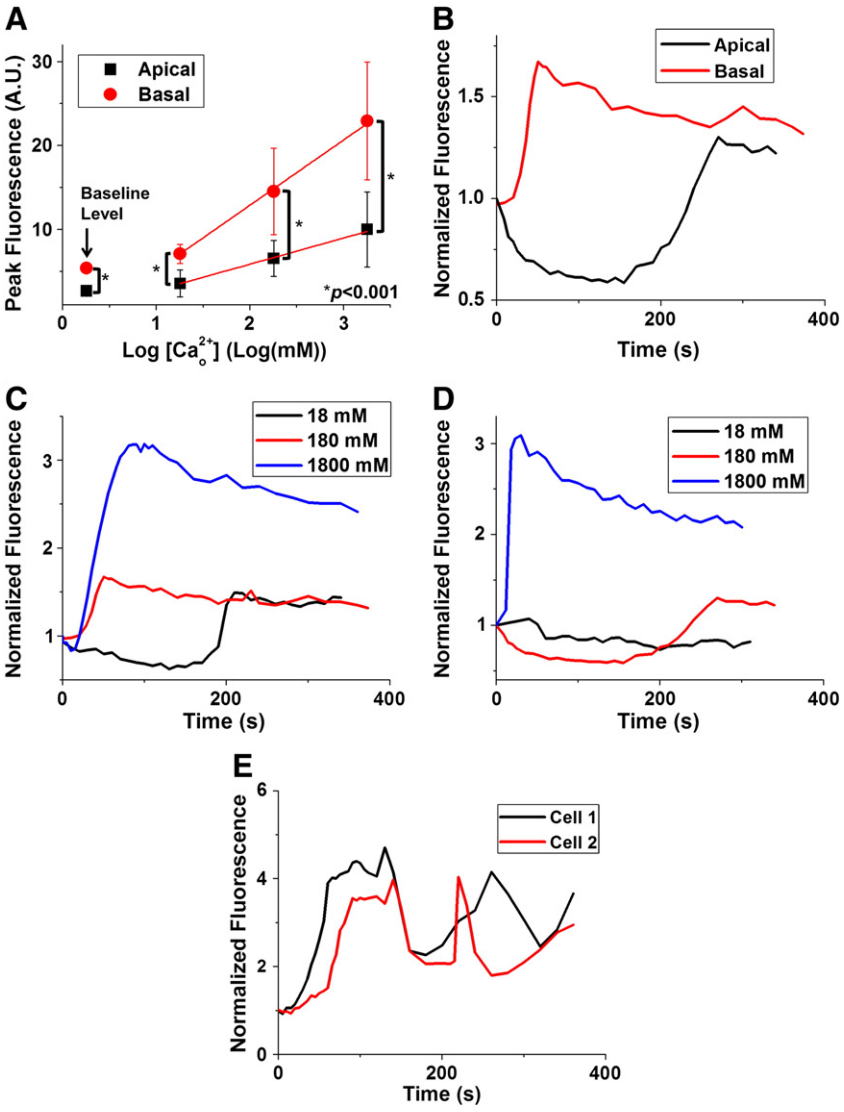

Fig. 7. Activation of MC3T3-E1 by mimicked Ca^{2+} efflux. (A) Peak fluorescence in cells at different extracellular Ca_o^{2+} levels in basal and apical groups. (B) Comparison of fluorescence increase in basal group and apical group at 180 mM Ca_o^{2+} level. (C) Comparison of fluorescence increase at three different levels of extracellular Ca_o^{2+} levels in basal group. (D) Comparison fluorescence increase at three levels of extracellular Ca_o^{2+} levels in apical group. (E) Representative curves for calcium (intracellular) oscillations (from 1800 mM basal group, similar oscillations observed in all three levels of extracellular Ca_o^{2+}).

3.4. Activation of bone cells by Ca^{2+} efflux: Efflux from the basal vs. apical aspects of the cell

Cell-seeded insert experiments showed that the intracellular Ca^{2+} level in MC3T3-E1 cells increased in response to the mimicked Ca^{2+} efflux in a dose-dependent manner, and the fluorescence intensity was proportional to the logarithm of the $\mathbf{[Ca_o^{2+}]}$ added either from underneath the porous substrate (basal group) or from above the cells (apical group) (Fig. 7A). Linear regression of the cellular fluorescence versus log$\mathbf{[Ca_o^{2+}]}$ was significant both for the basal group ($R^2 = 0.63$, P-value$<10^{-7}$) and the apical group ($R^2 = 0.43$, P-value$<10^{-6}$). Therefore, the extracellular calcium concentration $\mathbf{[Ca_o^{2+}]}$ is significantly associated with the activation level of intracellular calcium. Although cells in both groups responded to the extracellular $\mathbf{[Ca_o^{2+}]}$ gradient, the mean value of peak fluorescence intensity in the basal-group was twice the value of the apical-group, and this difference was significant ($P<0.001$) on all three levels of applied $\mathbf{[Ca_o^{2+}]}$ (Fig. 7A). It was also observed that the baseline fluorescence (before $CaCl_2$ was added) in the cells seeded on the porous inserts was higher than that in the cells seeded on the culture wells (Fig. 7A). In addition, the time needed for activation differed between the two groups: at the 180 mM $\mathbf{[Ca_o^{2+}]}$ level, cells subjected to calcium diffusion from the basal aspect responded immediately, while cells stimulated from the apical aspect were not activated until 4 minutes after the extracellular $\mathbf{[Ca_o^{2+}]}$ was applied (Fig. 7B). For the 18 mM level, cells in the basal group were activated at around 200 seconds, while cells in the apical group did not respond within the 5 minute recording time (Figs. 7C, D). At the 1800 mM level, cells in both groups were activated immediately upon stimulation (Figs. 7C, D). Oscillations in the cellular fluorescence were also observed at all levels of $\mathbf{[Ca_o^{2+}]}$ level (Fig. 7E).

3.5. Activating cells with osmotic pressure: glucose- vs. calcium-supplemented media

Upon the application of the supplemented medium in the insert group (basal stimulation from underneath the insert), we observed that the intracellular calcium response in the glucose-supplemented group ($F_{increase}/F_{baseline}$: 59% ± 29%, N = 10) was significantly less ($p = 0.02$) than that of the $CaCl_2$-supplemented group ($F_{increase}/F_{baseline}$: 105% ± 47%, N = 10), even though the two media had the same osmotic pressure. For the osteoblast-seeded culture well group, the intracellular calcium fluorescence increase upon stimulation in the glucose-

supplemented group ($F_{increase}/F_{baseline}$: 38% ± 22%, N = 10) was also significantly less ($p<0.001$) than that of the $CaCl_2$-supplemented group ($F_{increase}/F_{baseline}$: 70% ± 27%, N = 10),

4. Discussion

These results are the first to demonstrate that calcium efflux colocalizes with damage creation in bone matrix and osteoblasts seeded on bone substrates may respond to the efflux during *in vitro* mechanical testing by activating intracellular calcium signaling. Such a mechanism, if present *in vivo*, may act as a stimulus to cells to initiate repair cascade when strains are sufficiently large to induce microdamage.

The nature of the damage occurring in this model was characterized in our earlier work which demonstrated that stain uptake at the opaque zone was associated with the creation of positively charged void space in the order of magnitude of tens of nanometers [10,11]. This study confirmed the exposure of ionized calcium by using calcium indicators. Calcium ions are the most abundant source of positive charge in bone and these ions are associated with mineral crystals (intrafibrillar and extrafibrillar) [24] and highly phosphorylated non-collagenous proteins (mainly extrafibrillar) [8]. Current results indicated that Ca^{2+} efflux originates from damaged sites at both extrafibrillar and intrafibrillar spaces (Fig. 4).

Calcium microelectrode experiments indicate that Ca^{2+} dissociates from the surface of bone upon mechanical loading in unsupplemented phosphate buffered saline (PBS). Furthermore, the dissociation seems to be a diffusion-driven process, since when PBS was supplemented with 2 mM Ca^{2+} (the proposed Ca^{2+} concentration in the interstitial fluid of bone [25]), calcium efflux was diminished. While the lack of cellular response in demineralized bone strongly suggests the involvement of calcium efflux, the absence of strain induced efflux at calcium supplemented solutions requires explanation. First, the microelectrode cannot approach the surface of bone closer than 5 microns; therefore, absence of efflux in supplemented solutions at this level does not eliminate the possibility that an efflux is taking place at closer distances (i.e. within 1 micron of bone surface). Second, while damage appears homogenous at the macroscale (Fig. 4A), it appears discretely at the microscale (Fig. 4C) [10], and exact placement of microelectrode on a location undergoing damage is challenging. If we were able to place the electrode more accurately and more closely on individual damage entities as they happen, we may have possibly recorded efflux in the supplemented conditions as well. Since our results indicate that cells respond to calcium efflux more readily at the basal aspect in comparison to apical aspect, methods need to be developed to probe efflux at even closer distances than had been conducted here. The reduction in efflux with calcium supplementation indicates that the Ca^{2+} efflux is due to the dissolution and diffusion of calcium moieties which are exposed by damage processes. Surface bound bone cells (active and quiescent osteoblasts), are observed to attach tightly on bone matrix [26]. Therefore, there is a sealed compartment between cell membrane and bone matrix which might have a different Ca^{2+} concentration compared to that of the bulk interstitial fluid concentration. For instance, the space between osteoclast basal cell membrane and bone matrix reach concentrations as high as 40 mM [27]). While our results are suggestive, whether or not the reported matrix damage elevates the calcium concentration in the compartment between the basal aspect of cells and the matrix remains to be determined conclusively.

The concentrations of the extracellular $\mathbf{Ca_o^{2+}}$ applied in the mimicked Ca^{2+} efflux experiments (such as 180 mM and 1800 mM), were much higher than physiological level (about 40 mM in osteoclast resorption site [27]). We resorted to such concentrations in order to test if there is a logarithmic relationship between $\mathbf{[Ca_o^{2+}]}$ and the cellular response to because logarithmic relationship implies the involvement of voltage gated channels. Nevertheless, cells treated with highest $\mathbf{[Ca_o^{2+}]}$ in this study (1800 mM) still displayed "intracellular calcium oscillations" (Fig. 7E), which indicated that cells were viable under such supraphysiological $\mathbf{Ca_o^{2+}}$ level during the lifetime of the experiment (~5 minutes).

Local calcium concentration changes at observed Ca^{2+} efflux rates can be approximated by assuming 1-D diffusion from a semi-infinite plate. Assuming the height of the compartment between the cells and the bone surface to be in the 20 nm range [28] and the Ca^{2+} efflux as 2 pmol $cm^{-2}\,s^{-1}$ based on our experimental measurements, the observed efflux of calcium from bone can increase the concentration in that volume at a speed of 1 mM per second. Such steep increases in extracellular Ca^{2+} concentration has been shown by various studies to activate various bone cells [15,29,30]. Furthermore, in the calculation of the Ca^{2+} efflux from bone, we assumed 1-D diffusion from a semi-infinite plate, while the calcium indicator experiment suggested that the source of Ca^{2+} diffusion is more locally confined (Fig. 4B), and therefore, the Ca^{2+} efflux value is conservatively estimated here. In addition, although an ultrafine electrode was used to measure the Ca^{2+} concentration and efflux at the bone surface, the actual Ca^{2+} concentration which the seeded osteoblasts experienced is still unclear due to the fact cell attachment can get much closer to the bone surface than the electrode (20 nm vs. 5 micron) [28].

A potential source of calcium efflux is dissociation of Ca^{2+} from the exposed mineral crystals when the organic phase is debonded from the mineral phase under mechanical loading [7]. Such exposure of crystal would increase dissolution. Pure hydroxyapatite crystals have an equilibrium [Ca^{2+}] of ~50 μM in solution at pH = 7.4 [31], a value which is 50-fold greater than the [Ca^{2+}] measured at the bone surface at the baseline unloaded state. Therefore, crystal debonding from the organic coating during matrix damage formation can potentially lead to the increased calcium efflux by increasing the net surface area. Furthermore, composite mechanics models indicate that the stiff mineral crystals experience stresses up to GPa range [32] and such high stresses may increase solubility of crystals by way of providing energy to the dissolution process.

Calcium bound to the non-collagenous proteins (NCP) in the interfibrillar space may be another source for the efflux we observed. NCPs include a large number of phosphorylated amino acid side chains (such as PO_4^{3-} groups in phosphoserine and phosphothreonine), which bind to Ca^{2+} to form ion-bridges. It has been proposed that the glue-like NCP phase stretches during mechanical loading and the internal Ca^{2+} ion-bridges may be broken [8]. The density of PO_4^{3-} groups in NCPs was reported to be around 10 mM in bone [33]. Assuming that every two PO_4^{3-} can form an ion-bridge with one Ca^{2+}, the NCP phase binds to about 5 mM Ca^{2+} in bone. Once these ion-bridges are broken upon mechanical loading, the Ca^{2+} released from such NCP reservoir might also contribute to the elevated Ca^{2+} level observed in this study at bone surface, as it is calculated that NCP-bound Ca^{2+} in just a 3.6 μm layer of bone alone will be sufficient to sustain the level of Ca^{2+} efflux from bone for 20 min time period observed in this study (Fig. 5). Therefore, both crystal dissolution due to debonding between mineral and organic phases, and, Ca^{2+} release from NCP might contribute in the Ca^{2+} efflux observed in this study.

We also showed that osteoblasts near the stress concentrator on bone samples were activated as reflected by the elevation of intracellular $\mathbf{[Ca_i^{2+}]}$. $\mathbf{Ca_i^{2+}}$ is known to cascade into secondary mechanotransduction pathways that can lead to bone modeling and remodeling [34]. To determine whether such cellular response was due to mechanically-induced Ca^{2+} efflux or substrate deformation, we repeated the experiment with demineralized bone sample as well as the mimicked Ca^{2+} efflux with insert to rule out substrate deformation effect. The results demonstrated that mechanically-induced Ca^{2+} efflux rather than substrate deformation is the cause for cell activation observed in this study. Other studies have suggested that it takes at

least 800% strain to trigger certain mechanotransduction pathways in bone cells [35], and these magnitudes are too high to occur *in vivo*. Current results suggest that the Ca^{2+} efflux upon loading might be a potential signal to bone cells to trigger damage repairing, particularly in regions of bone subjected to stress amplification.

While the cell attachment was comparable between undemineralized and demineralized samples (Figs. 6A, B), demineralization alters the stiffness of the bone substrate, so at this stage we cannot rule out the consequence of such matrix stiffness alterations on the cell response to stretch. In addition, the load level applied in this study is in the spectrum of damage-level, it is uncertain that if normal physiological strain level will induce a Ca^{2+} efflux which is stimulatory to the bone cells. Therefore, our observations potentially apply more strongly to damaging level strains and less likely to bone adaptation at habitual strain levels. Cell-matrix interactions may have confounded the results when bone substrate is compared to insert experiments. While the cell-seeded PET insert is optimized for cell adhesion, the insert lacks the ECM-like environment, such as that presented by bone-slices. Therefore, the involvement of and ECM-like environment in bone-slices may have defined the observations we report to an unknown extent. Lastly, the loading regime in this study involved a single episode of stretching to induce Ca^{2+} efflux. However, repeated loading is more physiologically relevant (and more likely to induce damage at lower strains due to repetition), therefore, future studies will be investigating the effects of repeated loading at lower amplitude on calcium release and cell response.

In addition to MC3T3-E1 cells, we repeated these experiments on mouse primary osteoblasts (a gift from Dr. F. Pavalko, Indiana University) which also responded to the mimicked Ca^{2+} efflux in a dose-dependent manner in the absence of substrate stretch (data not shown).The promptness of cell response when stimulated from the basal region suggests that the receptors or channels involved in sensing the extracellular calcium are congregated in the basal region where the cell is attached to the substrate. Conversely, the lag in the response time for stimulation from the apical aspect (most evident in Fig. 7B) suggests fewer receptors or channels in the apical aspect or the lag is merely due to a delayed Ca^{2+} leakage into the space underneath the cell (basal side) when Ca^{2+} was applied from the apical side. In addition, we have shown a difference between the basal side versus the apical side in terms of the amplitude of cells' response to the changing $\mathbf{[Ca_o^{2+}]}$ level. The greater baseline fluorescence for cells seeded on porous inserts than regular culture wells suggested that exposing the basal side of the cells facilitates calcium detection. This might be similar to the observation that epithelial cells of the kidney predominantly express their Ca^{2+} sensing receptors (CaR) at their basolateral side [36]. In summary, such polarity in the response between the two sides of the cells indicates that cells might preferentially express their $\mathbf{[Ca_o^{2+}]}$ sensing receptors or channels on the basal side toward the substrate where cell attachment occurs. In this way, their ability to sense the calcium efflux from the bone may be maximized.

The logarithmic relationship between cellular response and applied extracellular $\mathbf{[Ca_o^{2+}]}$ suggests that the involved calcium sensing mechanism might be associated with the Ca^{2+} potential across the cell membrane which is proportional to the logarithm of the extracellular $[Ca^{2+}]$:

$$E = 2.303\frac{RT}{zF}\log\left(\frac{\left[Ca_{out}^{2+}\right]}{\left[Ca_{in}^{2+}\right]}\right)$$

where E is the membrane potential, R is the universal gas constant, T is the absolute temperature, z is the number of charges per molecule, and F is the Faraday's constant. One category of ion channels that seem fit such a relationship is the voltage-gated calcium channels (VGCC) [22,37]. VGCC are proposed to be activated by charged species in fluid flow [22,37], in which the cellular response is similar to what was observed in this study, including "intracellular calcium oscillations" (Fig. 7E) [21,38]. Therefore, these results suggest that the cellular response to the elevated extracellular $[Ca^{2+}]$ level might be caused by the difference in the membrane potential of $[Ca^{2+}]$, and this difference is likely to be sensed by VGCC preferentially located at the cell attachment side toward the bone substrate.

In addition to VGCC, calcium detection may occur via G protein-coupled $\mathbf{Ca_o^{2+}}$-sensing receptors (CaR) in osteoblasts, whose genes are similar to those found in parathyroid and kidney cells [41,42]. The presence of CaR mRNA and expression has been reported in both MC3T3-E1 osteoblast cell line [43,44] and *in situ* in bone slices [45]. Future studies targeting these receptors and channels are needed to identify the underlying mechanisms of the sensing of the calcium efflux from bone matrix by bone cells observed in this study.

Calcium efflux local to cells can potentially alter the osmotic pressure around the osteoblasts. Such changes in osmotic pressure might also be responsible for activating the cell by stretch-activated calcium channel (SACC) [39,40]. To investigate whether such osmotic pressure caused the cellular response observed in the mimicked calcium efflux experiments, we also repeated the insert experiment with 540 mM glucose-supplemented media of osmotic pressure equivalent of the 180 mM $CaCl_2$ supplemented medium. Upon the application of the supplemented medium, we observed that the intracellular calcium fluorescence in the glucose group was only about 50% of the $CaCl_2$ supplemented groups (for both osteoblasts seeded on porous insert and culture well), even though the two media had the same osmotic pressure. Therefore, we conclude that the osmotic pressure contributes to the observed intracellular calcium response only partially. The osmotic effects may come into play by opening the stretch-activated calcium channel (SACC) to allow the influx of extracellular calcium into the cytoplasm of the osteoblast [39,40], but the total amplitude of intracellular calcium response elicited by the Ca^{2+} supplemented medium cannot be explained solely by the increase in the osmotic pressure.

Besides calcium ions, inorganic phosphate groups (PO_4^{3+}) also constitute the apatite lattice of the bone mineral crystal (Ca/P molar ratio ~1.6 [46]). Therefore, the mechanically induced Ca^{2+} efflux should also be accompanied by the dissociation of PO_4^{3+} from the crystal lattice if the source of the Ca^{2+} efflux observed in this study includes the mineral crystals in bone. Therefore, such simultaneous release of inorganic phosphate may also have regulatory effects on bone cells as it has been shown for other cell types [47,48].

5. Conclusions

These results imply that bone matrix acts as an intermediate mechanochemical transducer that converts the mechanical strain into a chemical signal in terms of the Ca^{2+} efflux, particularly at critically loaded regions of bone during a post-yield loading. Such mechanochemical Ca^{2+} release might serve as a cell-perceivable signal by locally increasing the extracellular Ca^{2+} concentration around cells (as highlighted in the working hypothesis schema in Fig. 8), as it has been shown *in vitro* that increased level of extracellular Ca^{2+} stimulates osteoblast differentiation [15] and modulates the secondary messenger systems in osteocytes [17]. If present *in vivo*, the mechanism suggested here may explain how bone cells can identify regions of bone in need of repair or augmentation.

Author contributions

X.S. contributed to the bone mechanical testing and staining, real-time Ca efflux measurement, and *in vitro* cell activation study, and wrote the majority of the manuscript. E.M. contributed to the real-time Ca^{2+} efflux measurement and manuscript writing and revision. V.K. contributed to cell culture work and *in vitro* cell activation

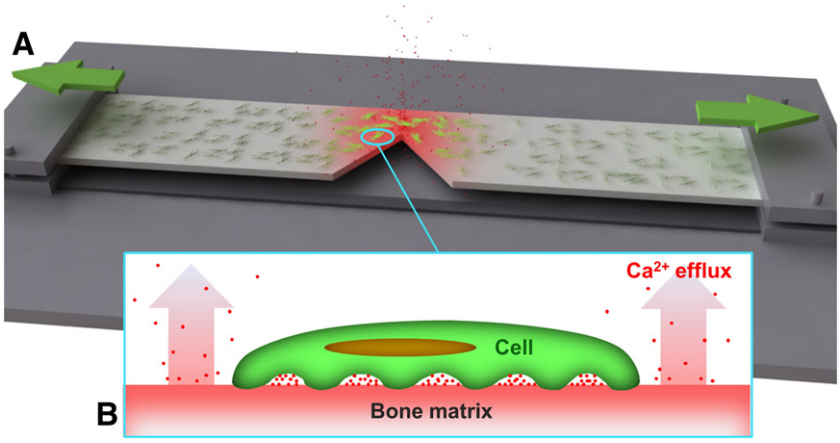

Fig. 8. Mechanotransduction via strain induced Ca^{2+} efflux from bone matrix. Bone matrix serves as the "mechanochemical transducer", converting mechanical loading into cell-perceivable chemical signals by perturbing extracellular calcium concentration during damaging mechanical load episodes. (A) Cell-seeded bone wafer subjected to tensile loading. Ca^{2+} (red particles) efflux from critically-loaded region on the notched bone specimen (white notched strip). Cells respond to increased pericellular Ca^{2+} around the notch (activated cells shown as bright green; non-activated cells shown as dark green). Direction of tensile loading is marked with green arrows. (B) Illustration of cross-sectional view of proposed Ca^{2+} efflux from cell-seeded bone substrate. Ca^{2+} ions (red particles) are more concentrated in the confined space between cell membrane and bone substrate on the cell attachment side than that in the open space.

study and manuscript revision. K.F. contributed to bone sample preparation and *in vitro* cell activation work. M.S. carried out SHG imaging and manuscript writing and revision. D.M.P. was involved in design and supervision of the Ca^{2+} efflux work. O.A. was involved in overall study design, supervision of the work and manuscript writing and revision.

Acknowledgments

This study was funded by NSF CAREER-0449188 (OA). The authors are grateful to Dr. Paul Hansma for the discussion on non-collagenous proteins as a potential source for Ca^{2+} efflux and to Dr. Eric Gruenstein for constructive critique of the manuscript. We acknowledge W. Scott Van Dyke for proofreading the manuscript and Michel J Schweinsberg for preparing Fig. 8.

References

[1] Zioupos P, Currey JD. The extent of microcracking and the morphology of microcracks in damaged bone. J Materials Sci 1994;29:978–86.
[2] Reilly GC, Currey JD. The effects of damage and microcracking on the impact strength of bone. J Biomech 2000;33:337–43.
[3] O'Brien FJ, Taylor D, Lee TC. Microcrack accumulation at different intervals during fatigue testing of compact bone. J Biomech 2003;36:973–80.
[4] Taylor D, Hazenberg JG, Lee TC. Living with cracks: damage and repair in human bone. Nat Mater 2007;6:263–8.
[5] Verborgt O, Gibson GJ, Schaffler MB. Loss of osteocyte integrity in association with microdamage and bone remodeling after fatigue in vivo. J Bone Miner Res 2000;15:60–7.
[6] Hazenberg JG, Freeley M, Foran E, Lee TC, Taylor D. Microdamage: A cell transducing mechanism based on ruptured osteocyte processes. J Biomech 2006;39:2096–103.
[7] Gupta HS, Seto J, Wagermaier W, Zaslansky P, Boesecke P, Fratzl P. Cooperative deformation of mineral and collagen in bone at the nanoscale. Proc Natl Acad Sci U S A 2006;103:17741–6.
[8] Fantner GE, Hassenkam T, Kindt JH, Weaver JC, Birkedal H, Pechenik L, et al. Sacrificial bonds and hidden length dissipate energy as mineralized fibrils separate during bone fracture. Nat Mater 2005;4:612–6.
[9] Tai K, Ulm FJ, Ortiz C. Nanogranular origins of the strength of bone. Nano Lett 2006;6:2520–5.
[10] Sun XH, Jeon JH, Blendell J, Akkus O. Visualization of a phantom post-yield deformation process in cortical bone. J Biomech 2010;43:1989–96.
[11] Xu ZB, Sun XH, Liu JJ, Song QH, Muckley M, Akkus O, et al. Spectroscopic visualization of nanoscale deformation in bone: interaction of light with partially disordered nanostructure. J Biomed Opt 2010;15:060503.
[12] Sherwood LM, Mayer GP, Ramberg CF, Kronfeld DS, Aurbach GD, Potts JT. Regulation of Parathyroid Hormone Secretion - Proportional Control by Calcium Lack of Effect of Phosphate. Endocrinology 1968;83:1043–51.
[13] Ebashi S, Endo M. Calcium ion and muscle contraction. Prog Biophys Mol Biol 1968;18:123–83.
[14] Bean BP. Neurotransmitter Inhibition of Neuronal Calcium Currents by Changes in Channel Voltage Dependence. Nature 1989;340:153–6.
[15] Dvorak MM, Siddiqua A, Ward DT, Carter DH, Dallas SL, Nemeth EF, et al. Physiological changes in extracellular calcium concentration directly control osteoblast function in the absence of calciotropic hormones. Proc Natl Acad Sci U S A 2004;101:5140–5.
[16] Quarles LD. Cation sensing receptors in bone: A novel paradigm for regulating bone remodeling? J Bone Miner Res 1997;12:1971–4.
[17] Kamioka H, Miki Y, Sumitani K, Tagami K, Terai K, Hosoi K, et al. Extracellular Calcium Causes the Release of Calcium from Intracellular Stores in Chick Osteocytes. Biochem Biophys Res Commun 1995;212:692–6.
[18] Kamioka H, Sumitani K, Tagami K, Miki Y, Terai K, Hakeda Y, et al. Divalent-Cations Elevate Cytosolic Calcium of Chick Osteocytes. Biochem Biophys Res Commun 1994;204:519–24.
[19] Porterfield DM. Measuring metabolism and biophysical flux in the tissue, cellular and sub-cellular domains: Recent developments in self-referencing amperometry for physiological sensing. Biosens Bioelectron 2007;22:1186–96.
[20] Clapham DE. Calcium signaling. Cell 2007;131:1047–58.
[21] Berridge MJ. Inositol trisphosphate and calcium signalling mechanisms. Biochim Biophys Acta, Mol Cell Res 2009;1793:933–40.
[22] Chen NX, Ryder KD, Pavalko FM, Turner CH, Burr DB, Qiu JY, et al. Ca2+ regulates fluid shear-induced cytoskeletal reorganization and gene expression in osteoblasts. Am J Physiol Cell Physiol 2000;278:C989–97.
[23] Huo B, Lu XL, Hung CT, Costa KD, Xu QB, Whitesides GM, et al. Fluid Flow Induced Calcium Response in Bone Cell Network. Cell Mol Bioeng 2008;1:58–66.
[24] Landis WJ. Structural relations between collagen and mineral in bone as determined by high voltage electron microscopic tomography. Microsc Res Tech 1996;33.
[25] Rasmusse P. Concentration of Calcium, Inorganic Phosphate and Protein in Interstitial Fluid of Rats. Calcif. Tissue Res 1970;6:197–203.
[26] Norimatsu H, Vanderwiel CJ, Talmage RV. Morphological Support of a Role for Cells Lining Bone Surfaces in Maintenance of Plasma Calcium Concentration. Clin Orthop 1979:254–62.
[27] Silver IA, Murrills RJ, Etherington DJ. Microelectrode Studies on the Acid Microenvironment beneath Adherent Macrophages and Osteoclasts. Exp Cell Res 1988;175:266–76.
[28] Miller SC. The Bone Lining Cell - a Distinct Phenotype. Calcif Tissue Int 1987;41:1–5.
[29] Yamaguchi T, Chattopadhyay N, Kifor O, Sanders JL, Brown EM. Activation of p42/44 and p38 Mitogen-Activated Protein Kinases by Extracellular Calcium-Sensing Receptor Agonists Induces Mitogenic Responses in the Mouse Osteoblastic MC3T3-E1 Cell Line. Biochem Biophys Res Commun 2000;279:363–8.
[30] Ye CP, Yamaguchi T, Chattopadhyay N, Sanders JL, Vassilev PM, Brown EM. Extracellular calcium-sensing-receptor (CaR)-mediated opening of an outward K+ channel in murine MC3T3-E1 osteoblastic cells: Evidence for expression of a functional CaR. Bone 2000;27:21–7.
[31] Mcdowell H, Gregory TM, Brown WE. Solubility of $Ca_5(PO4)_3OH$ in the system $Ca(OH)_2$-H_3PO_4-H_2O at 5, 15, 25, and 37 °C. J Res Nbs a Phys Ch 1977;81:273–81.
[32] Akkus O. Elastic deformation of mineralized collagen fibrils: An equivalent inclusion based composite model. J Biomech Eng-T Asme 2005;127:383–90.
[33] Cohensolal L, Lian JB, Kossiva D, Glimcher MJ. Identification of Ortho-Phosphothreonine in Soluble Non-Collagenous Phosphoproteins of Bone Matrix. FEBS Lett 1978;89:107–10.
[34] Chen JH, Liu C, You LD, Simmons CA. Boning up on Wolff's Law: Mechanical regulation of the cells that make and maintain bone. J Biomech 2010;43:108–18.

[35] Charras GT, Williams BA, Sims SM, Horton MA. Estimating the sensitivity of mechanosensitive ion channels to membrane strain and tension. Biophys J 2004;87:2870–84.
[36] Riccardi D, Hall AE, Chattopadhyay N, Xu JZ, Brown EM, Hebert SC. Localization of the extracellular Ca2+ polyvalent cation-sensing protein in rat kidney. Am J Physiol Renal 1998;274:F611–22.
[37] Li JL, Duncan RL, Burr DB, Turner CH. L-type calcium channels mediate mechanically induced bone formation in vivo. J Bone Miner Res 2002;17: 1795–800.
[38] Berridge MJ, Galione A. Cytosolic Calcium Oscillators. FASEB J 1988;2:3074–82.
[39] Miyauchi A, Notoya K, Mikuni-Takagaki Y, Takagi Y, Goto M, Miki Y, et al. Parathyroid hormone-activated volume-sensitive calcium influx pathways in mechanically loaded osteocytes. J Biol Chem 2000;275:3335–42.
[40] Hung CT, Allen FD, Pollack SR, Brighton CT. Intracellular Ca2+ stores and extracellular Ca2+ are required in the real-time Ca2+ response of bone cells experiencing fluid flow. J Biomech 1996;29:1411–7.
[41] Brown EM, MacLeod RJ. Extracellular calcium sensing and extracellular calcium signaling. Physiol Rev 2001;81:239–97.
[42] Hinson TK, Damodaran TV, Chen J, Zhang X, Qumsiyeh MB, Seldin MF, et al. Identification of putative transmembrane receptor sequences homologous to the calcium-sensing G-protein-coupled receptor. Genomics 1997;45: 279–89.
[43] Yamaguchi T, Chattopadhyay N, Kifor O, Butters RR, Sugimoto T, Brown EM. Mouse osteoblastic cell line (MC3T3-E1) expresses extracellular calcium (Ca-0(2+))-sensing receptor and its agonists stimulate chemotaxis and proliferation of MC3T3-E1 cells. J Bone Miner Res 1998;13:1530–8.
[44] Kanatani N, Sugimoto T, Kanzawa N, Yano S, Chihara K. High extracellular calcium inhibits osteoclast-like cell formation by directly acting on the calcium-sensing receptor existing in osteoclast precursor cells. Biochem Biophys Res Commun 1999;261:144–8.
[45] Chang YH, Tu CL, Chen TH, Komuves L, Oda Y, Pratt SA, et al. Expression and signal transduction of calcium-sensing receptors in cartilage and bone. Endocrinology 1999;140:5883–93.
[46] Cassella JP, Garrington N, Stamp TC, Ali SY. An electron probe X-ray microanalytical study of bone mineral in osteogenesis imperfecta. Calcif Tissue Int 1995;56:118–22.
[47] Jono S, McKee MD, Murry CE, Shioi A, Nishizawa Y, Mori K, et al. Phosphate regulation of vascular smooth muscle cell calcification. Circ Res 2000;87:E10–7.
[48] Seshagiri PB, Bavister BD. Glucose and Phosphate Inhibit Respiration and Oxidative-Metabolism in Cultured Hamster 8-Cell Embryos - Evidence for the Crabtree Effect. Mol Reprod Dev 1991;30:105–11.